

Sigma models on curved space and bubble refraction in doped antiferromagnets

J.M. Speight

School of Mathematics, University of Leeds, Leeds LS2 9JT, UK

Abstract

The dynamics of bubble solitons in two-dimensional isotropic antiferromagnets, inhomogeneously doped so that the exchange integral J becomes position dependent, is studied. In the usual continuum approximation, the system reduces to a nonlinear sigma model on a spacetime whose geometry depends on $J(x)$. It is shown, both within the geodesic approximation, and by appealing to field theoretic conservation laws, that a bubble incident on a domain wall inhomogeneity undergoes refraction in accordance with Snell's law, J^{-1} being identified with the refractive index, and that sufficiently oblique impacts result in total internal reflection. Possible applications of this phenomenon to the construction of bubble lenses and bubble guides (in analogy with fibre-optic cables) are considered.

1 Introduction

Topological solitons have important applications in many branches of physics, especially condensed matter and high energy physics. It often happens that the same soliton can be given completely different physical interpretations in these two disciplines, which has led in recent years to a very fruitful exchange of ideas and techniques. One of the most surprising and least exploited of these soliton correspondences is that between the isotropic Heisenberg antiferromagnet and the relativistic $O(3)$ sigma model. In this paper we will exploit this correspondence to show, using techniques from particle theory and differential geometry, that the trajectories of bubble-like solitons in inhomogeneously doped two-dimensional antiferromagnets experience refraction in exact analogy with Snell's law of refraction in geometric optics.

The isotropic Heisenberg antiferromagnet consists of an infinite square lattice of classical spin variables $S_{ij} \in \mathbb{R}^3$, with $\|S_{ij}\|^2 = s^2$, evolving according to the law

$$\frac{dS_{ij}}{dt} = -S_{ij} \times \frac{\partial H}{\partial S_{ij}}; \quad H = \sum_{i,j} J_{ij} (2s^2 + S_{ij} \cdot (S_{j+1,j} + S_{i+1,j})) \quad (1)$$

where t is time and $J > 0$ is a constant called the exchange integral. Note that since $J > 0$, H is minimized when each spin anti-aligns with its nearest neighbours. It is a curious fact that this dynamical system, first order in time and with an obvious preferred reference frame, can be described, in the continuum limit, by a Lorentz invariant PDE which is second order in time, namely

$$\partial_t n \cdot \partial_t n = 0; \quad \partial_t n = \frac{\partial^2 n}{\partial t^2} - J^2 \left(\frac{\partial^2 n}{\partial x^2} + \frac{\partial^2 n}{\partial y^2} \right) \quad (2)$$

where $n : \mathbb{R}^{2+1} \rightarrow \mathbb{R}^3$ has $\|n\|^2 = 1$, and t is a rescaled time variable. Note that (2) holds if and only if $\partial_t n$ is parallel to n , and hence

$$\partial_t n \cdot (\partial_t n - (n \cdot \partial_t n)n) = 0; \quad (3)$$

which is the more familiar form of the $O(3)$ sigma model (or wave map) equation. The connexion between n and S_{ij} is subtle, and will be explained in the next section. Roughly speaking, one should imagine the field n sampled on a square lattice, partitioned into black and white sublattices, chess-board fashion. The white spins evolve as $sn(t)$, the black as $-sn(t)$.

Imagine now that the antiferromagnet is inhomogeneously doped, so that the exchange integral becomes a function of position, $J(x;y)$. We will argue that the spin dynamics is now described by a field obeying

$$n \frac{\partial^2 n}{\partial t^2} - J(x;y)^2 \left(\frac{\partial^2 n}{\partial x^2} + \frac{\partial^2 n}{\partial y^2} \right) = 0; \quad (4)$$

which is the O(3) sigma model equation on spacetime \mathbb{R}^2 equipped with an inhomogeneous Lorentzian metric

$$= dt^2 - \frac{1}{J(x;y)^2} (dx^2 + dy^2); \quad (5)$$

Note that the static field equation is independent of J , so the usual Belavin-Polyakov lumps of the homogeneous system [3], which we shall call bubbles in this context (in analogy with magnetic bubbles in ferromagnets), carry over unchanged to the doped system. In this paper we make a detailed study of the dynamics of a single bubble in various inhomogeneous antiferromagnets, primarily within the geodesic approximation of Manton [4]. The main calculational task in this approach is to compute the metric on the one-bubble moduli space. This metric does depend on $J(x;y)$, and we obtain exact expressions for it for several interesting choices of this function.

Our main conclusion is that bubble trajectories experience refraction, in exact analogy with geometric optics, $J(x;y)^{-1}$ playing the role of the refractive index of the medium. The incident and exit angles of a bubble crossing a domain-wall J -inhomogeneity, for example, are related by Snell's law, and total internal reflection occurs if the impact is sufficiently oblique. This key observation is rederived without reference to the geodesic approximation by appealing to field theoretic conservation laws. We go on to study simple prototype bubble "lenses" and bubble guides, which use total internal reflection to guide bubble trajectories just as fibre optic cables guide light beams.

The rest of the paper is structured as follows. In section 2 we derive the PDE (4) from (1). In section 3 the geodesic approximation to the dynamics of a single bubble is set up. The interaction of a bubble with a domain wall is studied in 4 and Snell's law of refraction obtained. Sections 5 and 6 consider simple lenses and bubble guides respectively, while 7 presents some concluding remarks.

2 Doped antiferromagnets in the continuum limit

The spin lattice of interest is defined by (1), but with J replaced by a position dependent exchange integral, J_{ij} , so

$$\frac{dS_{ij}}{dt} = J_{ij} S_{ij} (S_{i+1,j} + S_{i-1,j} + S_{i,j+1} + S_{i,j-1}); \quad (6)$$

Following [1], to obtain a well-defined continuum limit for this system we, think of it as a lattice of dimers, that is, spin pairs. First, partition the square lattice chess-board fashion into black and white sublattices, with site $(i;j)$ white (black) if $i+j$ is even (odd). Associate to each white site $(i;j)$ the dimer consisting of $(S_{ij}; S_{i,j+1})$. The white sites can be labelled by a pair of (unconstrained) integers $(\alpha; \beta) = (i+j)=2; (i-j)=2$. We then call the two spins of the dimer $A = S_{ij}$ and $B = S_{i,j+1}$. Note that, while A lives on the white lattice and B on the black, both sets of variables are labelled with reference to the white lattice. Their evolution is governed by

$$\frac{dA}{dt} = J_{\alpha; \beta} (B_{\alpha; \beta+1} + B_{\alpha+1; \beta} + B_{\alpha-1; \beta} + B_{\alpha; \beta-1}); \quad (7)$$

$$\frac{dB}{dt} = J_{\alpha; \beta+1} (A_{\alpha+1; \beta} + A_{\alpha+1; \beta+1} + A_{\alpha-1; \beta+1} + A_{\alpha; \beta}); \quad (8)$$

We now think of the original $(i;j)$ lattice as having spacing $a > 0$, small, so that the $(\alpha; \beta)$ lattice has spacing $a = \frac{1}{2}$, and assume that A , B and J_{ij} have well defined continuum limits $A(\alpha; \beta)$, $B(\alpha; \beta)$ and $J(\alpha; \beta)$, where $\alpha = \frac{i+j}{2}$, $\beta = \frac{i-j}{2}$, so that $A_{\alpha+1; \beta} = A(\alpha; \beta) + a \frac{\partial A}{\partial \alpha} + \dots$, and so on. Note that $J(\alpha; \beta) = J_{\alpha; \beta}$, so

$$J_{\alpha; \beta+1} = J(\alpha + \frac{1}{2}; \beta + \frac{1}{2}) = J(\alpha; \beta) + \frac{1}{2} (J_{\alpha+1; \beta} + J_{\alpha-1; \beta}) + \frac{1}{8} (J_{\alpha+1; \beta+1} + J_{\alpha-1; \beta+1} + J_{\alpha+1; \beta-1} + J_{\alpha-1; \beta-1}) + \dots; \quad (9)$$

Substituting into (7), (8) and discarding terms of order ϵ^3 or higher, one obtains

$$2s \dot{A}_t = JA [4B - 2(B + B) + 2(B + B + B)] \quad (10)$$

$$2s \dot{B}_t = JB [4A + 2(A + A) + 2(A + A + A)] \\ B - [2(J + J)A + 2(J + J)(A + A) + \frac{2}{2}(J + J + 2J)A]; \quad (11)$$

where $t = 2s$ is a rescaled time variable.

These equations simplify somewhat if we introduce the auxiliary fields

$$m = \frac{1}{2s}(A + B); \quad n = \frac{1}{2s}(A - B); \quad (12)$$

Note that $m - n = 0$ and $j^2 + j^2 = 1$. Since we expect neighbouring spins to almost anti-align, m should be small, so we will assume, consistently with (10), (11), that $j = O(\epsilon)$, whence $j = 1 + O(\epsilon^2)$. Then, again neglecting terms of order higher than ϵ^2 , one finds

$$m_t = (\partial_x + \partial_y)[Jm - n] + \frac{1}{4}[2Jn - (n + n + n) + (J + J)n - (n + n)] \quad (13)$$

$$n_t = 4Jm - n - Jn - (n + n) - (J + J)m - n - \frac{2}{4}(J + J)n - (n + n); \quad (14)$$

Equation (14) may be solved for m ,

$$m = -\frac{1}{4}n - n_t - n - n + O(\epsilon^2); \quad (15)$$

which may then be substituted into equation (13). One finds that all the terms involving derivatives of J miraculously cancel, and

$$n - n_{tt} = J^2 n - (n + n) + O(\epsilon); \quad (16)$$

To leading order, therefore, n is governed by the $O(3)$ sigma model equation on R^2 with metric $dt^2 + (dx^2 + dy^2) = J^2(\cdot, \cdot)$, which is (4) up to relabelling. It is slightly more natural, however, to define continuum position variables $x = i\epsilon$, $y = j\epsilon$ aligned with the original spin lattice, rather than \cdot , aligned with the white sublattice. Since the x, y coordinates are obtained from \cdot by a rotation (through 45), $\partial^2 + \partial^2 = \partial_x^2 + \partial_y^2$, so we again obtain (4), but with $J(x, y) = J_{ij}$. To reconstruct the actual spin dynamics, given a solution of (4), we must choose $\epsilon > 0$ small, construct the auxiliary field m from (15),

$$m = -\frac{\epsilon}{2} \frac{1}{2} n - n_t - n_y; \quad (17)$$

extract A and B , then sample these on the white and black sublattices, respectively, of the lattice of spacing ϵ .

The above derivation is closely modelled on that of Komineas and Papanicolaou [1], so we have omitted some of the details of the calculation. The main difference is that we have included the extra terms due to the position dependence of J . In the end, all these extra terms cancel, to leading order, and we are left with the continuum PDE one would have first guessed on naive grounds. This is somewhat surprising, and it would be satisfying to have a more direct argument for it than the rather complicated derivation given here.

3 The geodesic approximation

Equation (4) is the variational equation for the action

$$S = \frac{1}{2} \int dt dx dy \left(\frac{1}{J(x, y)^2} \left(\frac{\partial n}{\partial t} \right)^2 - \frac{1}{2} \left(\frac{\partial n}{\partial x} \right)^2 + \frac{1}{2} \left(\frac{\partial n}{\partial y} \right)^2 \right) \quad (18)$$

where

$$T = \frac{1}{2} \int dx dy \frac{1}{J(x, y)^2} \left(\frac{\partial n}{\partial t} \right)^2; \quad V = \frac{1}{2} \int dx dy \left(\frac{\partial n}{\partial x} \right)^2 + \left(\frac{\partial n}{\partial y} \right)^2. \quad (19)$$

are identified as the kinetic and potential energy functionals respectively. Note that while T depends on J , V does not. Hence Belavin's and Polyakov's analysis of the static homogeneous model [3] carries over unchanged to the doped system. There is a topological lower energy bound

$$V[n] \geq 4\pi j; \quad (20)$$

m being the topological degree of the map $n: R^2 \rightarrow S^2$. Let us define complex coordinates $z = x + iy$ on the spatial plane and $u = (n_1 + in_2)/(1 - n_3)$ on the target sphere (the latter being the image of n under stereographic projection from $(0,0,1)$ to the equatorial plane). Then the bound (20) for $m = 0$ is attained if and only if $u(z)$ is a rational map of algebraic degree m . Since such rational maps minimize V (globally within their homotopy class, in fact) they are automatically stable static solutions of the model. If we choose the boundary value of n at spatial infinity to be $(0,0,1)$, the general degree 1 bubble is

$$u(z) = e^{i\theta} \frac{(z - a)}{2} =: u_0(z; \theta; a); \quad (21)$$

$\theta \in [0, 2\pi)$, $a \in \mathbb{C}$ and $a = a_1 + ia_2 \in \mathbb{C}$ being constants interpreted as the bubble's width, internal phase and position respectively.

Following Ward [5] and Leese [6], we will study the low energy dynamics of a single bubble within the geodesic approximation of Manton [4]. The idea is that M_1 , the four dimensional space of static bubbles, parameterized by $\theta; a_1; a_2$, which we will denote collectively as q^i , is a flat valley bottom in the space of all degree 1 maps $R^2 \rightarrow S^2$, on which V attains its minimum value of 4. If a bubble is given a small amount of kinetic energy, its subsequent motion is confined close to M_1 by conservation of energy $E = T + V$, suggesting that a collective coordinate approximation wherein the motion is constrained to M_1 for all time is sensible. So we assume that

$$u(z; t) = e^{i\theta(t)} \frac{(z - a(t))}{2}; \quad (22)$$

substitute (22) into S , and obtain variational equations for $\theta; a$. Note that $V = 4$, constant, for all fields of the form (22), and T is quadratic in time derivatives, so the action reduces to

$$S = \frac{1}{2} \int dt g_{ij} \dot{q}^i \dot{q}^j; \quad g_{ij}(q) = \frac{1}{J(x; y)^2} \frac{4}{(1 + |u_0(z; q)|^2)^2} \frac{\partial u_0}{\partial q^i} \frac{\partial u_0}{\partial q^j}; \quad (23)$$

which is the action for geodesic motion on M_1 with respect to the metric $g = g_{ij}(q) dq^i dq^j$. The conceptual framework and validity of this approximation are discussed at length in [7].

The metric g , and hence the dynamics, depends strongly on $J(x; y)$. If J is constant, we are studying the standard sigma model, and it is found that θ and a are frozen by infinite inertia ($g_{\theta\theta} = g_{aa} = 1$) and $g_{zz} = 4/J^2 da da$, so bubbles just travel at constant velocity [5]. At the other extreme, if $J(x; y) = 1 + x^2 + y^2$, we effectively have the sigma model on a round two-sphere, and the bubble dynamics is much richer [8]. This choice has J unbounded, which is presumably unphysical, however. If we assume that J remains bounded, then θ and a are frozen by an essentially identical argument to Ward's. Without loss of generality, we can set $\theta = 0$. The width a remains a free, but frozen, parameter. The metric on M_1 , the width, phase 0 leaf of M_1 , is then

$$g = f(a) (da_1^2 + da_2^2); \quad (24)$$

where

$$f(a) = \frac{1}{J(z; z)^2} \frac{4}{(1 + |u_0(z; a)|^2)^2} = \frac{1}{J(u + a)^2} \frac{4}{(1 + |u_0|^2)^2}; \quad (25)$$

the integral of $J(u + a)^{-2}$ over the standard unit sphere, u being a stereographic coordinate. If J is sufficiently simple, $f(a)$ can be computed explicitly. Note that

$$\lim_{a \rightarrow 0} g = \frac{4}{J(a)^2} (da_1^2 + da_2^2); \quad (26)$$

which is the bubble rest mass, $M = 4/J(a)^2$, times the inhomogeneous metric on the physical plane. In the limit of vanishing width, therefore, bubble trajectories tend to geodesics, not just in M_1 , but also in the physical plane. One may regard g as a smeared out version, due to the bubble's finite core size, of the metric on physical space.

4 Domain walls

The simplest and most experimentally feasible type of inhomogeneous doping is the domain wall. Let us assume that J depends only on x , is constant outside a small neighbourhood of $x = 0$ and rises monotonically from J to J_+ as x traverses this neighbourhood. Such a $J(x)$ would arise from doping one end of an antiferromagnet but not the other. If the domain wall is very narrow, we may idealize it by a step function,

$$J(x) = \begin{cases} J_+ & x \geq 0 \\ J & x < 0 \end{cases} \quad (27)$$

Then from (25) we see that f depends only on a_1 and

$$f(a_1) = \frac{A}{J^2} + \frac{4}{J_+^2} \frac{A}{J_+} \quad (28)$$

where A is the area of $S \subset S^2$, the region on which $\text{Re}(u + a) < 0$. The stereographic image of S is the half-plane to the left of the straight line $u_1 = -a_1$. The corresponding boundary curve $\partial S \subset S^2$ is a circle whose diameter (in the metric space sense) is the length of any great circular arc lying in S , intersecting ∂S orthogonally. One such arc has stereographic image $z = i \tan \frac{1}{2} \theta$ for $\theta \in [\pi/2, 3\pi/2]$. The geometry of the situation is depicted in figure 1. Hence

$$\text{diam}(S) = \int_{-1}^1 \frac{2}{1+t^2} dt = 2 \tan^{-1} \frac{a_1}{J_+} \quad (29)$$

To compute the area of any disk in S^2 with diameter diam , we can use spherical polar coordinates with the "North pole" placed at the centre of the disk. Then

$$A(\text{diam}) = \int_0^{2\pi} \int_0^{\frac{1}{2}\text{diam}} \sin \theta d\theta d\phi = 2\pi \left(1 - \cos \frac{1}{2}\text{diam}\right) \quad (30)$$

Together, (28), (29) and (30) yield

$$f(a) = \frac{2}{J^2} \left(1 - \frac{a_1}{2 + a_1^2}\right) + \frac{2}{J_+^2} \left(1 + \frac{a_1}{2 + a_1^2}\right) \quad (31)$$

Note that, despite the discontinuity in J , f is smooth, and that f is a decreasing function of a_1 with $\lim_{a_1 \rightarrow \infty} f(a_1) = 4/J^2$. If J is smoothed around $x = 0$, these properties, on which we will base all our dynamical arguments, persist, although the exact formula (31) is lost.

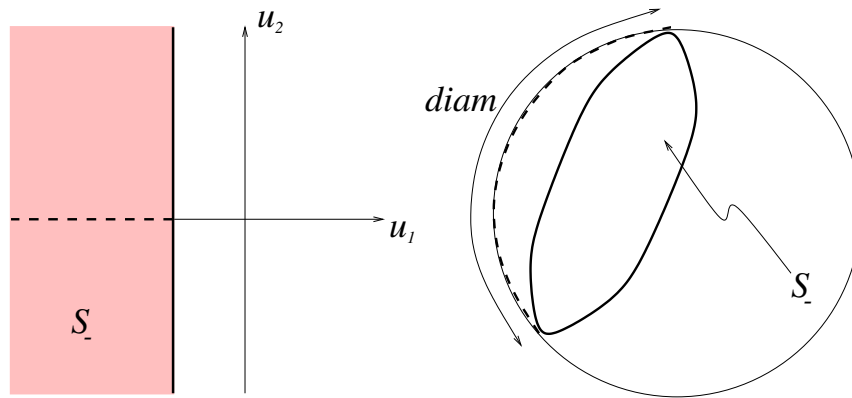


Figure 1: The region $S \subset S^2$ defined in the derivation of f , equation (31), right, and its stereographic image, left. The dashed curve is the great circular arc whose length is the metric space diameter of S .

To analyze geodesic flow in M_1 , we note that the Lagrangian governing $a(t)$ is $L = \frac{1}{2} f(a_1)(\dot{a}_1^2 + \dot{a}_2^2)$. The time evolution conserves both energy $e = L$ and the momentum conjugate to a_2 , $p_2 = f(a_1)\dot{a}_2$. Since geodesic trajectories are independent of initial speed, we may set $E = 1$. Then

$$1 = \frac{1}{2} f(a_1) \dot{a}_1^2 + \frac{p_2^2}{2f(a_1)} \quad (32)$$

for all time. Consider a bubble \vec{a} incident obliquely at the domain wall from the left, that is, with $a_1(0) < 0$, $\dot{a}_1(0) > 0$, $\dot{a}_2(0) \neq 0$. Since $f(a_1)$ is decreasing, $a_1(t)$ must have a turning point if $|p_2|$ (hence $|\dot{a}_2(0)|$) is too large, else (32) is violated. Hence a bubble which hits the wall with too large an incidence angle is reflected from it, just like a light ray undergoing total internal reflection. In fact, the analogy with refraction is much deeper. Let us assume that the incident bubble has velocity $v(\cos \theta; \sin \theta)$ as $t \rightarrow 1^-$, $\theta = 2 < \theta < \pi/2$, so that it impinges on the wall, and is transmitted with velocity $v_+(\cos \theta_+; \sin \theta_+)$ as $t \rightarrow 1^+$. Then by conservation of e and p_2 ,

$$\frac{2}{J_+^2} v_+^2 = \frac{2}{J^2} v^2 \quad \text{and} \quad \frac{4}{J_+^2} v_+ \sin \theta_+ = \frac{4}{J^2} v \sin \theta \quad (33)$$

whence one sees that

$$\frac{1}{J_+} \sin \theta_+ = \frac{1}{J} \sin \theta : \quad (34)$$

This is precisely Snell's law of refraction, where we identify J^{-1}, J_+^{-1} as the refractive indices of the materials on either side of the wall. Hence, total internal reflection occurs if

$$|\sin \theta| > \sin^{-1}(J/J_+) : \quad (35)$$

Note that (34) is independent of θ , as it must be, since the sharp domain wall $J(x)$ is invariant under dilation of the physical plane $(x; y) \mapsto (\lambda x; \lambda y)$. It is straightforward to solve the geodesic equations for $g = f(a_1)(\dot{a}_1^2 + \dot{a}_2^2)$ numerically and confirm the behaviour predicted. Figure 2 depicts bubble scattering off a sharp domain wall with $J_+ = J_- = 2$ at a range of incidence angles.

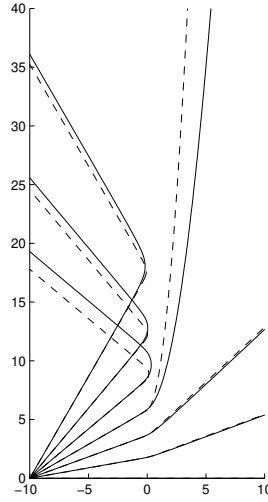


Figure 2: Scattering of bubbles of width $\epsilon = 0.5$ (solid curves) and width $\epsilon = 0.1$ (dashed curves) off a domain wall, in the geodesic approximation. The region to the left of the vertical line $x = 0$ has $J = J_- = 1$, while that to the right has $J = J_+ = 2$. Note that bubbles are reflected if their incidence angle exceeds 30° , in accordance with Snell's law.

Although we have derived Snell's law within the framework of the geodesic approximation, one can rederive it using only field theoretic conservation laws. By Noether's theorem and t and y translation invariance, the

full field theory conserves $E = T + V$ and

$$P_z = \int dx dy \frac{1}{J(x)^2} \frac{\partial n}{\partial t} \frac{\partial n}{\partial y} : \quad (36)$$

The key point is that the effective spacetime metric is, except in a narrow strip containing the y -axis, the Minkowski metric, but with the "speed of light" differing on either side of the wall. Given a static solution strongly localized in one of the two flat regions, therefore, we can produce (almost) exact moving solutions by an appropriate Lorentz boost. Let $n_0(x; y)$ be the static bubble given by $u(z) = \frac{1}{J} z$. The boosted bubble with velocity $v = (\cos \theta; \sin \theta)$,

$$n_-(t; x; y) = n_0((x \cos \theta - y \sin \theta - vt); x \sin \theta + y \cos \theta); \quad (37)$$

where the contraction factor is $\gamma = (1 - v^2 = J^2)^{-\frac{1}{2}}$, tends to an exact solution as $t \rightarrow \pm \infty$. Using this as initial data at $t = -\infty$, let us consider the field's subsequent evolution. Presumably the bubble impinges on the domain wall. Let us assume that the bubble is transmitted, and that its interaction with the wall is elastic, so no energy is lost to radiation. Then, as $t \rightarrow \infty$ it is once again a free bubble moving at constant velocity, so must approach some translate of

$$n_+(t; x; y) = n_0((x \cos \theta + y \sin \theta - vt); x \sin \theta + y \cos \theta); \quad (38)$$

with contraction factor $\gamma_+ = (1 - v_+^2 = J^2)^{-\frac{1}{2}}$. It is straightforward to compute E and P_z for n_+ as $t \rightarrow \infty$, yielding the conservation laws

$$M_+ = M_- \quad \text{and} \quad \frac{v_+ + \sin \theta}{J_+^2} M_+ = \frac{v - \sin \theta}{J^2} M_-; \quad (39)$$

where $M_- = 4$ is again the rest energy of the bubble, which together imply (34). Note that M_- is independent of θ , so this argument holds even if the interaction with the wall somehow changes the bubble's width. The limiting factor on the applicability of (34) is thus the assumption of elastic scattering off the wall, which one expects to hold at small incidence velocities, rather than the validity of the geodesic approximation itself.

5 Circular lenses

It is interesting to consider the interaction of bubbles with curved domain walls. The observation that bubbles undergo refraction, with J^{-1} identified as the refractive index, immediately gives a simple "geometric optics" model of their trajectories, which should hold whenever the bubble width is large relative to the domain wall width, but small relative to its radius of curvature. This raises the interesting possibility that lenses can be constructed which could be used to focus bubbles onto a target area. Such a lens would consist of a thin region bounded by a pair of circular arcs of large radius, within which J is suppressed relative to its value outside the region. This is a rather complicated choice of $J(x; y)$ for the purposes of computing g , so we shall here test the feasibility of antiferromagnetic lenses more indirectly, by studying the scattering of bubbles off complete disks of suppressed J , for which g can again be computed explicitly. Clearly, such circular "lenses" are far from the thin lenses used for focussing in optics. Nevertheless, by comparing bubble trajectories incident on a circular lens with their geometric optics analogues, we can provide strong evidence that bubble focussing is possible.

We shall again make a thin domain wall approximation, so that $J(z)$ is piecewise constant, taking one value on some disk and another value elsewhere. By conformal invariance we can, without loss of generality, assume the disk has unit radius. Hence

$$J(z) = \begin{cases} J_- & |z| < 1 \\ J_+ & |z| \geq 1 \end{cases} \quad (40)$$

with $J_- < J_+$. We can again use formula (28), but now S^2 is the region on which $|ju + a| < 1$. This is again a disk, whose stereographic image is bounded by the circle of radius J_-^{-1} centred at $a = \frac{1}{J_-}$. By rotating

around the n_3 axis, this disk can be centred on the positive u_2 axis, so that the segment of this axis from $u_2 = (\tilde{a}j - 1) =$ to $u_2 = (\tilde{a}j + 1) =$ becomes a great circular arc in S intersecting ∂S orthogonally. Hence

$$\text{diam}(S) = \int_{(\tilde{a}j-1)}^{(\tilde{a}j+1)} dt \frac{2}{1+t^2} = 2 \tan^{-1} \frac{\tilde{a}j+1}{1} - \tan^{-1} \frac{\tilde{a}j-1}{1}; \quad (41)$$

which, together with (30) and (28) gives

$$f(a) = \frac{2}{J^2} \left[1 - \sqrt{\frac{2 + \tilde{a}j^2 - 1}{4 + 2\tilde{a}j^2(\tilde{a}j^2 + 1) + (\tilde{a}j^2 - 1)^2}} \right] + \frac{2}{J_+^2} \left[1 + \sqrt{\frac{2 + \tilde{a}j^2 - 1}{4 + 2\tilde{a}j^2(\tilde{a}j^2 + 1) + (\tilde{a}j^2 - 1)^2}} \right]; \quad (42)$$

Note that f depends on $\tilde{a}j$ alone, is smooth, and has $\lim_{\tilde{a}j \rightarrow 1} f(a) = 4/J_+^2$, as one would expect. The dependence on the bubble width cannot, as in the case of a straight sharp domain wall, be scaled away. Unless $\tilde{a}j = 1$, therefore, we should expect bubble trajectories to diverge significantly from their optical analogues.

For sufficiently large $\tilde{a}j > 1$ (0.17 if $J_+ = J_- = 2$), $(M_1; g)$ may be isometrically embedded as a surface of revolution in R^3 , using the method described in [9]. Figure 3 shows numerically generated generating curves for these surfaces of revolution for various values of χ : the surfaces themselves are swept out as the curves are rotated about an axis vertical in the page. It is not surprising that the isometric embedding fails for small $\tilde{a}j$. Recall that in the limit $\tilde{a}j \rightarrow 0$, g tends to a multiple of the metric on the physical plane, which for this choice of J is clearly singular. It can be roughly visualized as the flat plane with the unit disk cut out, expanded by a linear factor of $J_+ = J_-$, its edge then re-attached to the hole. The surfaces depicted in Figure 3 are on the way to this geometry as $\tilde{a}j$ gets small. An interesting point to note is that a pinched neck develops in the surface for $\tilde{a}j < \tilde{a}j_2$ (0.36 for $J_+ = J_- = 2$). The two circles swept out by the points where the tangent to the curve is vertical are both geodesics. Hence there is a bifurcation in the geodesic flow at $\tilde{a}j = \tilde{a}j_2$, a pair of periodic geodesics appearing as $\tilde{a}j$ is reduced through $\tilde{a}j_2$. Although we have deduced the existence of these periodic geodesics visually, it is easy to show that they exist for all $\tilde{a}j < \tilde{a}j_2$ (even if $\tilde{a}j < 1$, so that no isometric embedding exists) by appealing to conservation of energy e and angular momentum $p = f(\tilde{a}j)\tilde{a}j^2$, where $a = \tilde{a}j^2$. The corresponding bubble trajectories are circular orbits centred on $z = 0$, one inside the disk and one just outside. Such trajectories have no optical analogue.

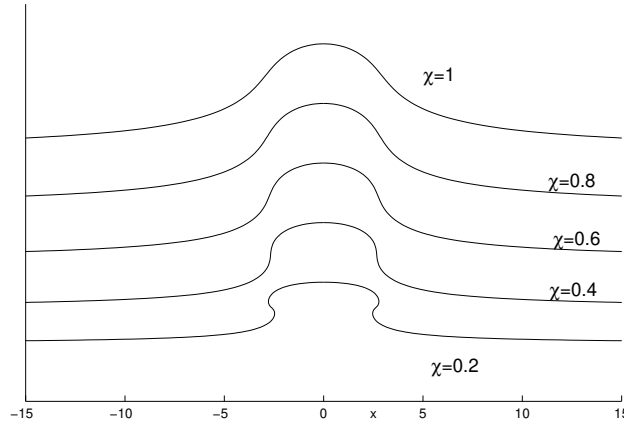


Figure 3: Generating curves for M_1 isometrically embedded as a surface of revolution in R^3 for various χ , in the case of a sharp disk inhomogeneity with $J_- = 1$, $J_+ = 2$. The surfaces are swept out as these curves are rotated about the axis $x = 0$. Note that a neck develops as $\tilde{a}j$ becomes small.

It is again straightforward to solve the geodesic problem numerically. Figure 3 shows the scattering of bubbles initially moving along parallel trajectories for two different choices of $\tilde{a}j$. A focussing effect is apparent, and the trajectories look optical in the case of very narrow bubbles. To make a quantitative comparison, we present in Figure 4 plots of the exit angle of the bubble as a function of its impact parameter $b = \lim_{t \rightarrow 1} a_2(t)$

for a variety of widths χ , in comparison with the exit angle for light rays,

$$\theta_{\text{light}}(b) = 2 \sin^{-1} \frac{J}{J_+} b \sin^{-1} b : \quad (43)$$

Clearly, bubble scattering is increasingly optical as they become narrower, as one expects. Even for moderately narrow bubbles the geometric optics picture works well except for very glancing impacts (b close to 1). One area where the geometric optics model fails badly is scattering with b just exceeding 1. Light rays in this case miss the disk completely, so $\theta_{\text{light}}(b) = 0$. Bubbles, on the other hand, can become almost trapped by the neck in M_1 , and scatter with nontrivial θ , having wound several times around the disk. The dependence of θ on b is very sensitive in this regime, see figure 4.

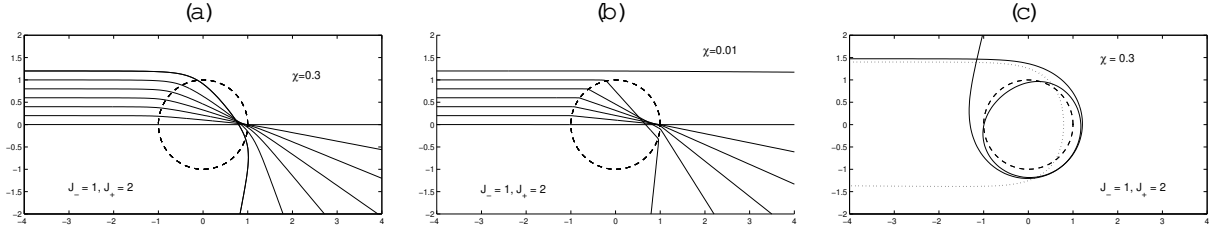


Figure 4: Scattering of bubbles off a circular "lens" with $J_+ = J_- = 2$: (a) and (b) show the expected focussing effect for $\chi = 0.3$ and 0.01 respectively, while (c) shows the sensitive dependence of the trajectory on its initial data when it winds around the neck of M_1 ($\chi = 0.3$ again).

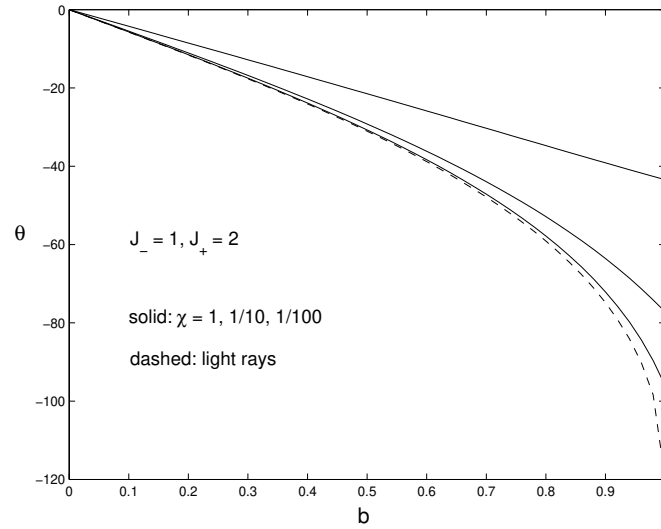


Figure 5: The exit angle of a bubble trajectory scattering off a circular lens with $J_+ = J_- = 2$, as a function of impact parameter for $\chi = 1, 0.1, 0.01$ (solid curves, top to bottom), in comparison with the exit angle for light rays (dashed).

If we choose $J > J_+$, the disk causes bubble trajectories to diverge rather than focus, as one would expect. Again the trajectories are increasingly optical as χ becomes small. A significant difference is that M_1 can never be isometrically embedded in R^3 , and there are no periodic geodesics.

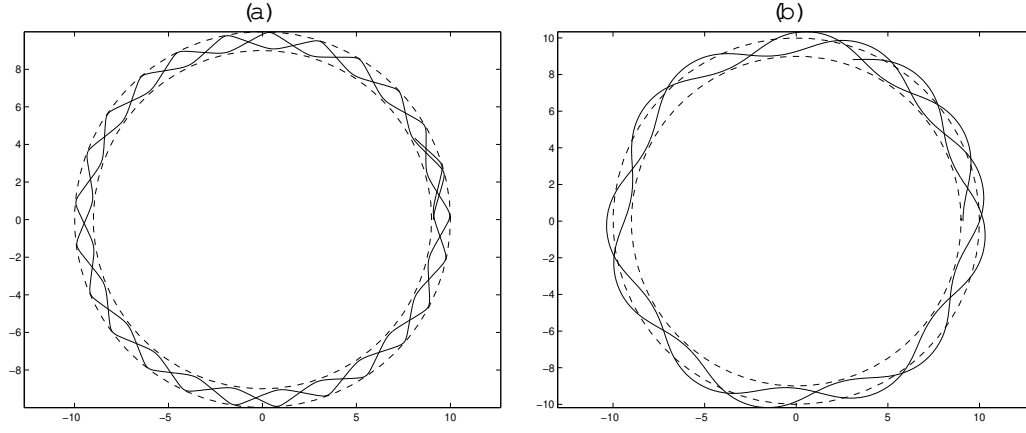


Figure 6: A circular bubble guide, analogous to a fibre optic cable. The region between the dashed circles has J suppressed by a factor of 2. Total internal reflection keeps narrow bubbles ($\epsilon = 0.1$) between the walls, (a). Even a bubble as wide as the track itself ($\epsilon = 1$) is guided along it, (b).

6 Bubble guides

The total internal reflection phenomenon might be used to construct the analogue for bubbles of fibre optic cables: doped tracks of low J in a high J substrate which would guide bubbles along a prescribed path. A simple example, for which $f(a)$ can still be obtained exactly, is an annular track with

$$J(z) = \begin{cases} J_- & r_1 < |z| < r_2 \\ J_+ & \text{elsewhere} \end{cases} \quad (44)$$

where $J_- < J_+$ as before. Once again (28) holds, but now S (or rather its stereographic image) is the annular region centred on $a=0$ bounded by radii r_1 and r_2 . The area of this region can be computed in similar fashion to the previous cases (by finding the diameters of its inner and outer disks), yielding the formula

$$f(a) = \frac{4}{J_+^2} + 2 \frac{1}{J_+^2} \frac{1}{J_-^2} [h(\tilde{a}; r_1) - h(\tilde{a}; r_2)]; \quad (45)$$

where

$$h(\tilde{a}; r) = \frac{r^2 + \tilde{a}^2 - \tilde{a}^2}{4 + 2\tilde{a}^2(\tilde{a}^2 + r^2) + (\tilde{a}^2 - r^2)^2}; \quad (46)$$

Bubble trajectories within such an annular bubble guide with $J_+ = J_- = 2$ and $r_1 = 9$, $r_2 = 10$, obtained numerically within the geodesic approximation, are depicted in figure 6. A narrow bubble ($\epsilon = 0.1$, compared with the track width of unity) initially moving within the annulus is trapped by the domain walls and guided around it. Even a bubble as wide as the track ($\epsilon = 1$) is guided along it, although the bubble centre now strays beyond the domain walls, and the trajectory looks far from optical.

7 Conclusion

We have argued that, in the near continuum regime, a two-dimensional isotropic Heisenberg antiferromagnet with inhomogeneous doping should be well modelled by the relativistic $O(3)$ sigma model on a spatially inhomogeneous spacetime. By conformal invariance, such a model supports static Belavin-Polyakov lumps, which we call bubbles. The trajectories of these bubbles are predicted to behave like light rays propagating in an inhomogeneous medium, with J^{-1} , the inverse exchange integral, identified with the refractive index. In particular, bubbles incident on a straight domain wall are refracted in accordance with Snell's law, and total internal reflection can occur. This result was derived both within the framework of the geodesic approximation,

and by appeal to field theoretic conservation laws. Its validity is not contingent on the validity of the geodesic approximation *per se*, but rather on the assumptions that the interaction of bubble and domain wall is elastic, which should certainly be true for low impact speeds, and that the scattering does not cause the bubble to collapse immediately (it must survive long enough to travel far from the domain wall for our conservation law argument to apply). Bubble collapse is an intense focus of current research, and it is still unclear whether collapse is generic.

In the present context, it would be perverse to try to settle this issue by lattice simulation of the sigma model, since this is itself merely an approximation to the more fundamental spin lattice (1). Numerical simulations of (1) seeking the refraction phenomena noted here are the logical next step, but lie beyond the scope of this paper. Even if bubble collapse does turn out to be a serious problem, there is still hope that bubble refraction may occur in real-life systems because, just as in the case of ferromagnets, higher order interactions may contribute extra terms which stabilize the bubble [10]. These terms destroy the conformal invariance of the sigma model, so there would be corrections to Snell's law due to the J dependence of the bubble's rest mass, but the basic refractive behaviour may persist. The main obstacle to seeing such refraction in a real antiferromagnet is that, since neighbouring spins almost anti-align, bubbles have almost zero magnetization, and are thus difficult to observe experimentally.

To illustrate the possibility, it is instructive to consider the spatially inhomogeneous system studied recently by Piette et al [11],

$$S = \int dt dx dy \frac{1}{2} (\partial_\mu n^\mu)^2 + \frac{1}{4} [(\partial_\mu n^\mu)^2 - (\partial_\mu n^\mu)^2] - \frac{(x;y)}{2} (1 - n_3^2); \quad (47)$$

which may be loosely interpreted as an antiferromagnet with homogeneous and isotropic exchange integral ($J = 1$), but with inhomogeneous on-site easy-axis anisotropy (the potential coefficient $(x;y)$ depends on position). This system supports approximate bubble type solutions, localized in regions of constant n , but their width is no longer a free parameter, and both their width and rest-mass now depend on position. Let us assume again that we have domain wall doping, so $(x;y) = -1$ for $x < 0$, $(x;y) = +1$ for $x > 0$. Then we expect the rest mass of a bubble in the right half-plane, M_+ , to exceed that of a bubble in the left half-plane, M_- (Piette et al find $M_+ = M_- + 1.029$ for $\alpha = 0.6$, $\alpha = 0.7$, for example). What happens when a bubble moving with speed v at incident angle θ hits the domain wall? By energy conservation, it must be reflected if $M_- < M_+$, independent of θ . Assume v exceeds this threshold, $v^2 > 1 - M_-^2/M_+^2$, and the bubble crosses the barrier, escaping with speed v_+ at angle θ_+ . Then energy conservation $M_- \gamma = M_+ \gamma_+$ gives v_+ as a function of v , and clearly $v_+ < v$. Again, the y -component of linear momentum is conserved, so $v \sin \theta = v_+ \sin \theta_+$, which together with energy conservation imply

$$v_+ \sin \theta_+ = v \sin \theta; \quad (48)$$

Since $v > v_+$ refraction does occur (the bubble bends away from the normal), and the bubble must undergo total internal reflection if θ exceeds the v -dependent Brewster angle $\sin^{-1} [v_+/(v) = v]$.

Turning to theoretical high energy physics, the $O(3)$ sigma model has long been a favoured model for those interested in soliton dynamics in geometrically exotic spacetimes [8, 12, 13, 14, 15, 16]. Our observation raises the possibility that some exotic spacetime may be artificially engineered in the laboratory. Furthermore, since Snell's law emerges from conformal invariance (the soliton's rest mass is independent of J) and very general conservation law arguments, soliton refraction should not be a special feature of this particular model. One would expect it to be a feature of Yang-Mills instanton dynamics in $4+1$ dimensions, for example.

Acknowledgements

The author thanks Stavros Komineas for helpful correspondence about antiferromagnets.

References

- [1] S. Komineas and N. Papanicolaou, "Vortex dynamics in 2D antiferromagnets" *Nonlinearity* 11 (1998) 265.
- [2] J. Shatah and C. Zeng, "Schrödinger maps and antiferromagnetic chains" to appear in *Commun. Math. Phys.*
- [3] A. A. Belavin and A. M. Polyakov, "Metastable states of two-dimensional isotropic ferromagnets" *JETP Lett.* 22 (1975) 245.
- [4] N. S. Manton, "A remark on the scattering of BPS monopoles" *Phys. Lett.* 110B (1982) 54.
- [5] R. S. Ward, "Slowly moving lumps in the CP^1 model in $(2+1)$ dimensions" *Phys. Lett.* 158B (1985) 424.
- [6] R. A. Leese, "Low energy scattering of solitons in the CP^1 model" *Nucl. Phys. B* 344 (1990) 33.
- [7] N. S. Manton and P. M. Sutcliffe, *Topological Solitons*, Cambridge University Press, Cambridge, UK, (2004) pp 102-108.
- [8] J. M. Speight, "Low energy dynamics of a CP^1 lump on the sphere" *J. Math. Phys.* 36 (1995) 796.
- [9] J. A. McGlade and J. M. Speight, "Slow equivariant lump dynamics on the two sphere" preprint hep-th/0503086 (2005).
- [10] A. S. Kirakosyan, V. L. Pokrovsky, "From Bubble to Skyrmion: Dynamic Transformation Mediated by a Strong Magnetic Tip" preprint cond-mat/0305487 (2003).
- [11] B. Piette, W. J. Zakrzewski and J. Brand, "Scattering of topological solitons on holes and barriers" preprint hep-th/0508032 (2005).
- [12] J. M. Speight, "Lump dynamics in the CP^1 model on the torus" *Commun. Math. Phys.* 194 (1998) 513.
- [13] J. M. Speight and I. A. B. Strachan, "Gravity thaws the frozen moduli of the CP^1 lump" *Phys. Lett.* 457B (1999) 17.
- [14] A. Comtet and G. W. Gibbons, "Bogomol'nyi bounds for cosmic strings" *Nucl. Phys. B* 299 (1988) 719.
- [15] N. M. Romão, "Dynamics of CP^1 lumps on a cylinder" *J. Geom. Phys.* 54 (2005) 42.
- [16] R. J. Cova and W. J. Zakrzewski, "Soliton scattering in the $O(3)$ model on a torus" *Nonlinearity* 10 (1997) 1305.